HHS Public Access

Author manuscript

*Neuron*. Author manuscript; available in PMC 2018 February 08.

Published in final edited form as:

*Neuron*. 2017 February 08; 93(3): 533–541.e5. doi:10.1016/j.neuron.2016.12.023.

# Tau Pathology Induces Excitatory Neuron Loss, Grid Cell Dysfunction and Spatial Memory Deficits Reminiscent of Early Alzheimer's Disease

**Hongjun Fu**[1,4], **Gustavo A. Rodriguez**[1,4], **Mathieu Herman**[1], **Sheina Emrani**[1], **Eden Nahmani**[1], **Geoffrey Barrett**[1], **Helen Y. Figueroa**[1], **Eliana Goldberg**[1], **S. Abid Hussaini**[1,2,4,5], and **Karen E. Duff**[1,2,3,5,6]

[1]Taub Institute for Research on Alzheimer's Disease and the Aging Brain, Columbia University Medical Center, New York, NY 10032, USA

[2]Department of Pathology and Cell Biology, Columbia University Medical Center, New York, NY 10032, USA

[3]Department of Integrative Neuroscience, New York State Psychiatric Institute, New York, NY 10032

## Summary

The earliest stages of Alzheimer's disease (AD) are characterized by the formation of mature tangles in the entorhinal cortex and disorientation and confusion navigating familiar places. The medial entorhinal cortex (MEC) contains specialized neurons called grid cells that form part of the spatial navigation system. Here we show in a transgenic mouse model expressing mutant human tau predominantly in the EC that the formation of mature tangles in old mice was associated with excitatory cell loss and deficits in grid cell function, including destabilized grid fields and reduced firing rates, as well as altered network activity. Overt tau pathology in the aged mice was accompanied by spatial memory deficits. Therefore, tau pathology initiated in the entorhinal cortex could lead to deficits in grid cell firing and underlie the deterioration of spatial cognition seen in human AD.

### Keywords

Tau pathology; Alzheimer's disease; entorhinal cortex; grid cells; neuronal loss; cognitive deficits; transgenic mouse model

Correspondence to: S. Abid Hussaini; Karen E. Duff.

[4]Co-first author

[5]Co-corresponding author

[6]Lead Contact

**Author Contributions**: This study was designed by K.E.D., H.F. and S.A.H. The manuscript was written by K.E.D., H.F. G.A.R and S.A.H. Experiments were performed by H.F., S.A.H., G.A.R., M.H., S.E., E.N., H.Y.F., and E.G. The data were analyzed by H.F., S.A.H, G.A.R., G.B. and K.E.D.

## Introduction

Neurofibrillary tangles (NFTs) composed of hyperphosphorylated and aggregated microtubule-associated protein tau (MAPT) are one of the hallmarks of Alzheimer's disease (AD) (Lee et al., 2001). In the earliest stages of AD, NFTs accumulate in the somatodendritic compartment of entorhinal cortex (EC) neurons, especially in layers II and III. They then spread into limbic and association cortices via the trisynaptic circuit in a precise and defined manner (Braak and Braak, 1991). Structural imaging studies demonstrate early and selective atrophy in the EC, which correlates with severe cell loss of more than 70% of layer II and 40% of layer III neurons (Braak and Braak, 1991; Gomez-Isla et al., 1996; Masdeu et al., 2005; Stranahan and Mattson, 2010), and hypometabolism in functional imaging studies (Khan et al., 2014). Thus the EC has been implicated as a primary site of dysfunction in the early stages of the disease.

Spatial navigation is known to be affected very early during AD (reviewed in (Lithfous et al., 2013), including in preclinical AD (Allison et al., 2016) and the EC is known to play an important role in spatial navigation (Fyhn et al., 2004; Jacobs et al., 2010; Moser et al., 2008). The medial EC (MEC) contains several classes of neurons with unique response characteristics, the best known being grid cells (Hafting et al., 2005; Igarashi, 2016; Kropff et al., 2015). Grid cells encode an animal's spatial location by selectively firing in a triangular grid-like pattern (grid fields) across an environment. Because of the location of tangle pathology in early AD, dysfunction in grid cell firing has been hypothesized to underlie symptoms of spatial disorientation in AD, including those at genetic risk of AD (Kunz et al., 2015).

We, and others have generated a transgenic mouse model (line EC-Tau) in which a highly aggregable form of *MAPT* is expressed predominantly in the hippocampal formation under the control of a neuropsin promoter fragment (Liu et al., 2012; de Calignon et al., 2012; Harris et al., 2012). Using this mouse model we demonstrate that the accumulation of tau pathology in the EC is associated with excitatory neuronal loss and grid cell dysfunction. Mice at this stage also show spatial learning and memory deficits. This is the first study showing a relationship between tau pathology and grid cell dysfunction *in vivo*, which may provide the link between tau pathology and spatial cognition deficits in early AD.

## Results

### Mature Tau Pathology is Associated with Spatial Memory Deficits in Aged EC-Tau Mice

We have previously shown that at younger ages (≤ 14 months), human tau in the EC-tau mouse line was diffuse and mainly distributed in axons with a few cells in the EC and parasubiculum (PaS) showing accumulation in the somatodendritic compartment (Liu et al., 2012). By 30+ mo of age, axonal staining in EC-Tau mice was almost completely lost, and human tau protein had accumulated extensively in cell bodies within the hippocampal and parahippocampal regions, as well as in extrahippocampal areas of the cortex (Figure 1A). There was negligible somatodendritic human tau staining in control mice (Figure S1A). To investigate whether mature tau pathology in aged mice could induce learning and memory deficits we compared EC-Tau and control mice at 14 and 30+ months of age by Morris water

maze (MWM) and T-maze tests. At 14 months of age, there were no significant learning and memory deficits in EC-Tau mice compared to matched controls (Figures 1B-1E), which is consistent with published data that showed EC-Tau mice at 16 months of age were cognitively normal (Harris et al., 2012; Polydoro et al., 2014). At 30+ months of age, however, there were significant differences between EC-Tau and control mice in escape latency ($P < 0.05$, 0.01 and 0.001 for Trial day 2-4, respectively) (Figure 1B), the number of platform crossings in the 2 h ($t = 3.693$, $df = 12$, $P = 0.0031$) (Figure 1C) and 24 h probe trial of MWM ($t = 3.083$, $df = 12$, $P = 0.0095$) (Figure 1D), and the percent correct choice in T-maze (*Chi-square* = 4.822, $df = 1$, $P = 0.0281$) (Figure 1E). In addition, there were significant differences in escape latency ($P < 0.001$ and $P < 0.05$ for Trial day 2 and 3, respectively) (Figure 1B) and the number of platform crossings in the 2 h ($t = 4.393$, $df = 15$, $P = 0.0005$) (Figure 1C) and 24 h probe trial of MWM ($t = 4.954$, $df = 15$, $P = 0.0002$) between control mice at 14 mo and control mice at 30+ mice (Figure 1D), with a trend to decrease that did not reach significance in the percent of correct choice in the T-maze (*Chi-square* = 0.8046, $df = 1$, $P = 0.3697$) in 30+ mo control mice (Figure 1E). However, the differences in escape latency ($P < 0.001$ for Trial day 2-4), the number of platform crossings in the 2 h ($t = 7.085$, $df = 14$, $P < 0.0001$) and 24 h probe trial of MWM ($t = 4.736$, $df = 14$, $P = 0.0003$), and the percent of correct choice in the T-maze (*Chi-square* = 6.513, $df = 1$, $P = 0.0107$) between EC-Tau mice at 14 mo and EC-Tau mice at 30+ mo were greater than the differences between controls at 14 and 30+ mo. Moreover, there was no significant difference in escape latency on Trial day 4 between control mice at 14 mo and control mice at 30+ mo, but a significant difference between EC-Tau mice at 14 mo and EC-Tau mice at 30+ mo ($P < 0.001$). Swim speed, visual ability and body weight were not significantly different between experimental groups at 14 and 30+ months of age (Figures S1B-1D), which suggests that the learning and memory deficits in aged EC-Tau mice were not attributable to abnormalities in sensorimotor function, visual acuity or body weight.

## Reduced Grid Cell Firing and Periodicity in the Dorsal MEC of Aged EC-Tau Mice

As the MEC is known to be involved in spatial learning and memory, we wanted to test whether tau pathology impacts the underlying physiology of MEC neurons. Multi-electrode *in vivo* electrophysiology was used to extracellularly record from neurons in the MEC of 14 mo and 30+ mo EC-Tau mice and age-matched controls (Figure 2). The animals were surgically implanted with 16-channel electrodes aimed at dorsal MEC (coordinates: 3.1mm lateral to lambda, 0.2mm in front of transverse sinus, angled at 6-8° posterior and 0.8mm below the surface of the brain. See Method Details of STAR Methods, “Electrode implantation and surgery”) (Figure S3C-D). The animals were then allowed to explore one of several open field arenas each day for two sessions as we recorded single unit and local field potentials (LFPs). Electrodes were turned no more than 50 μm each day to maintain stable recordings, and the electrophysiological data were analyzed to identify neuronal firing patterns and network activity (see Figure S2 and STAR Methods for Method details). A total of 434 excitatory neurons were recorded in 29 mice (for cell-type information see Method Details of STAR Methods, “*In vivo* recording and cell classification”). Grid cells were identified based on their grid-like firing patterns, and their spatial periodicity was calculated into a grid score for each cell. Grid scores were calculated for all cells and only those with positive grid scores were shuffled randomly to obtain 122 grid cells that exceeded the 95th

percentile threshold (Figure S3A). At 14 mo, we observed no difference in grid field patterns from EC-Tau mice compared to age-matched controls (Figure 2A). However, 30+ mo EC-Tau mice showed poor specificity of grid field patterns compared to other groups (Figure 2B). We observed reduced grid scores in 30+ mo EC-Tau mice compared to age matched controls (Figure 2C, left panel; $P < 0.0001$, Mann-Whitney $U$: 143.5) and histograms (30 bins) of grid score percentages showed clear separation of the 30+ mo EC-tau group from other groups (Figure 2C, right panel). Grid cells in the 30+ mo EC-Tau mice also exhibited reduced peak firing ($P < 0.0001$, Mann-Whitney $U$: 127.5) and average firing ($P = 0.0161$, Mann-Whitney $U$: 243.0) rates compared to age-matched controls (Figure 2D). In addition, the grid cells of 30+ mo EC-tau mice had reduced information content, measured in bits per second, compared to the aged controls (Fig. 3A, left panel; $P < 0.0001$, Mann-Whitney $U$: 146.5). We did not detect differences in grid cell information content between the 14-mo groups. There were no differences in spatial coherence of grid cells between age-matched groups (Fig. 3A, right panel). We also analyzed firing rates of other MEC cell types, including head-direction cells, border cells, and non-classified cells, but did not detect any differences in peak or average firing rates between age-matched EC-Tau mice and controls (Figure S5).

## Increased Interneuron Firing and Enhanced Power of Theta in the Dorsal MEC of Aged EC-Tau Mice

MEC interneurons are intricately connected to stellate and pyramidal cells, including grid cells. Thus, we examined whether firing properties of MEC interneurons were also altered in aged EC-Tau mice as a result of tau pathology. A total of 93 interneurons were recorded in 29 mice (for cell-type information see Method Details of STAR Methods, "*In vivo* recording and cell classification"). There were no significant differences in the proportion of interneurons recorded with respect to other cell-types in any age group ($P > 0.05$, see STAR Methods). Putative interneurons in the MEC were identified based on their narrow spike widths and higher firing rates compared to wide spiking cells (Quirk et al., 2009). We found the average firing rate of interneurons was increased in 30+ mo EC-Tau mice compared to age-matched controls ($P = 0.0193$, Mann-Whitney $U$: 142.5), with no effect between groups at 14-mo (Figure 3B). Peak firing rate was not affected in either group at any age. To investigate if the overall network activity in MEC was affected, local field potentials were also recorded and analyzed. We found an increase in power distribution in the theta frequency range (4-12 Hz) in 30+ mo EC-Tau mice compared to controls (Figures 3C-E, two-way ANOVA. $df = 717$ Interaction: $P < 0.0001$ $F = 18.98$, Genotype: $P < 0.0001$ $F = 25.14$ and Age: $P = 0.0323$ $F = 4.600$). There was no significant difference in power distribution in the gamma frequency range (35-55 Hz) for any groups. We found no differences between groups at any age in theta- or gamma-phase locked interneurons (data not shown).

## Excitatory but not Inhibitory Neurons are Vulnerable in Aged EC-Tau Mice

Significant neuronal loss was previously reported at 24 months of age (but not at 21 months of age) in the EC-II and PaS of EC-Tau mice compared to control mice (de Calignon et al., 2012). Consistent with this finding, we also found that the number of neurons ($NeuN^+$) in MEC-II ($P = 0.0079$) as well as MEC-III/IV ($P = 0.0018$) was significantly reduced in 30+

mo EC-Tau mice compared to control mice (Figure S4A). Thioflavin $S^+$ tau, indicative of mature tangles, was only observed in the EC and pre/parasubiculum (Figures S4B-4D) at 24 and 34 mo, with larger aggregates being observed at 34 mo. AT100 (a marker of AD-related hyperphosphorylated tau (Matsuo et al., 1994) labeled a larger set of neurons than Thioflavin S at younger ages but co-localized with Thioflavin $S^+$ tau at 30+ mo (Figures S4B-4D). To identify which type of cell accumulated pathological human tau, we performed sequential staining with antibodies against human tau ($MC1^+$), excitatory neurons ($TBR1^+$) and inhibitory neurons ($PV^+$ or $SOM^+$) (Belforte et al., 2010) in 30+ mo EC-Tau and control mice (Figure 4). The $MC1^+$-tau staining in the MEC was completely colocalized with $TBR1^+$ excitatory neurons, but not with $PV^+$ or $SOM^+$ inhibitory neurons (Figures 4A-4C, and 4E). Furthermore, the number of $TBR1^+$ excitatory neurons was significantly reduced in the MEC-II and MEC-III/IV in aged EC-Tau mice compared to matched controls ($P = 0.0022$) (Figure 4D). However, there was no difference in the number of $PV^+$ or $SOM^+$ inhibitory neurons between aged EC-Tau and control mice ($P > 0.05$) (Figure 4D).

## Discussion

In this study, we demonstrated that in aged EC-tau mice, pathological human tau accumulated in the somatodendritic compartment of cells in the hippocampal formation as well as in hippocampus proper and neocortical regions, and this was accompanied by spatial learning and memory deficits measured by the MWM and T-maze tests. EC-Tau mice at 30+ mo were more impaired than controls at 30+ mo, and mice with more severe pathology at 30+ mo were more impaired than EC-tau mice at 14 mo, which were not different from age-matched controls. At 30+ mo of age, control mice were impaired compared to control mice at 14 mo, but the EC-Tau mice at 30+ showed a greater deficit compared to 14 mo EC-tau mice. These results indicate that tau pathology contributes more than age effects to the spatial learning and memory deficits observed in aged EC-Tau mice.

Grid field size and grid field spacing has been shown to progressively increase along the MEC dorsoventral axis (Giocomo et al., 2011). Interestingly, dorsal MEC appears to be selectively vulnerable to pathological tau, and not ventral MEC, as shown by a recent study (Booth et al., 2016). With these key findings in mind, we targeted the dorsal MEC for *in vivo* recordings in our young and aged cohorts. We found a significant reduction in grid cell firing rates, grid scores, and spatial information content in 30+ mo EC-Tau mice, indicating impaired spatial representation in this cohort, reminiscent of early Alzheimer's disease. The increased number of low grid scores observed in these aged mice was not tied to low firing rates, as downsampling (two-fold) the data from young mice - which exhibited the highest firing rates -did not significantly affect grid scores (Figure S3B). Moreover, it has been previously shown that grid scores and mean vector length can both tolerate a high degree of downsampling without affecting either measure (Bonnevie et al., 2013). The reduced firing in excitatory grid cells and increased firing in inhibitory interneurons likely results in increased inhibitory constraint within the MEC, leading to enhanced power of theta, which is thought to be driven by increased activity of inhibitory neurons (Stark et al., 2013). Although grid cell periodicity is reduced by abolishing theta rhythms when the medial septum is inactivated (Brandon et al., 2011), there might be additional mechanisms involved that increase the power of theta in the EC-Tau mouse model. It is possible that accumulation

of tau specifically in MEC excitatory neurons combined with extensive neuronal loss causes theta to increase. The increase in theta power is consistent with enhanced theta rhythm seen in mild cognitive impairment and early AD (Jeong, 2004; Montez et al., 2009; Moretti et al., 2009; Siwek et al., 2015; Stam, 2010). We hypothesize that mature tauopathy mainly affects excitatory neurons but spares inhibitory neurons, causing cell death in the former and altering network activity.

Based on the altered firing properties of grid cells, inhibitory neurons and neural oscillations observed in aged EC-Tau mice, we propose that the accumulation of mature tangles may disturb the balance between excitatory and inhibitory neurons. NFTs have been identified in human AD brain in cells that, based on their morphology and location, were proposed to be excitatory (Hof et al., 2003). In order to investigate whether excitatory or inhibitory neurons are vulnerable to tau pathology, we first counted the number of total neurons in aged EC-Tau mice. The number of total neurons ($NeuN^+$) in MEC-II as well as MEC-III/IV was significantly reduced in 30+ mo EC-Tau mice compared to control mice. This is consistent with a previous finding on this mouse line that significant neuronal loss was reported at 24 months of age (but not at 21 months of age) in the EC-II and PaS of EC-Tau mice compared to control mice (de Calignon et al., 2012). Thioflavin $S^+$ tau, indicative of mature tangles, was only observed in the EC and pre/parasubiculum at 24 and 34 mo, with larger aggregates being observed at 34 mo. This suggests that overt cell death is only associated with mature tangles, although synapse loss and altered neuronal activity have been reported in the hippocampal regions in younger EC-Tau mice (de Calignon et al., 2012; Harris et al., 2012; Polydoro et al., 2014). To identify whether tau-positive cells were excitatory or inhibitory we performed immunohistochemistry co-localization studies. $MC1^+$-tau staining in the MEC was completely colocalized with $TBR1^+$ excitatory neurons, but not with $PV^+$ or $SOM^+$ inhibitory neurons. Further, the number of $TBR1^+$ excitatory neurons was significantly reduced in the MEC-II and MEC-III/IV in aged EC-Tau mice compared to matched controls. However, there was no difference in the number of $PV^+$ or $SOM^+$ inhibitory neurons between aged EC-Tau and control mice. These results suggest that pathological tau differentially impairs excitatory neurons compared to inhibitory neurons, which could cause the hypoexcitability observed in the MEC, resulting in destabilized grid fields.

Taken together, we have demonstrated that mature tau pathology in aged EC-tau mice leads to excitatory cell loss in the MEC, grid cell dysfunction and alterations in cell firing properties. While it is not possible to directly link these deficits in the MEC to the spatial memory deficits seen in aged EC-Tau mice due to pathology occurring in other regions in addition to the MEC, it is clear that tau pathology can cause spatial navigation deficits, which could explain the disorientation and navigation deficits seen in early human AD.

## Contact For Reagent and Resource Sharing

Further information and requests for reagents may be directed to, and will be fulfilled by the Lead Contact, Karen E Duff (ked2115@columbia.edu) at the Taub Institute for Research on Alzheimer's disease and the Aging Brain, Columbia University Medical Center.

## Experimental Model and Subject Details

We previously generated the line of tau transgenic mice known as EC-Tau (previously known as Neuropsin-tTA-Tau or NT; genotype: Tg(Klk8-tTA)SMmay/MullMmmh Tg(tetO-MAPT*P301L)#Kha/JlwsJ; strain background: FVB/N:C57BL/6) (Liu et al., 2012; Khan et al., 2014) by crossing the neuropsin-tTA "activator" line (genotype: Tg(Klk8-tTA)SMmay/MullMmmh; strain background: congenic on C57BL/6 background) (Yasuda and Mayford, 2006) with a tetracycline-inducible "responder" line (genotype: Tg(tetO-MAPT*P301L)#Kha/JlwsJ; strain background: FVB/N background) (Santacruz et al., 2005). The F1 offspring (both males and females, EC-Tau genotype or controls (non transgenic littermates from the EC-tau cross), strain FVB/N:C57BL/6) were used as experimental animals. All animals were maintained on a 12 h light/dark cycle with food and water provided ad libitum. All animal experiments were performed in accordance with national guidelines (National Institutes of Health) and approved by the Institutional Animal Care and Use Committee of Columbia University. The behavior tests were performed with two separate cohorts of naïve mice at 14 months and 30+ months of age during the light phase; neuronal activity was also recorded during the light phase. At each age, T-maze was performed first, followed by Morris water maze (MWM) two weeks later. If the animals died or were sick during, or before the final test, they were removed from the data analysis.

## Method Details

### Immunohistochemistry

Mice were transcardially perfused with phosphate-buffered saline (PBS) (Fisher Scientific, Fair Lawn, New Jersey, USA), brains were harvested and drop-fixed in 4% paraformaldehyde (PFA) (Electron Microscopy Sciences, Hatfield, PA, USA) in PBS at 4$^{o}$C overnight, followed by incubation in 30% sucrose (Sigma-Aldrich, Saint Louis, MO, USA) in PBS until the brains sank to the bottom of the container. Brains were sectioned (35 μm) throughout on a horizontal plane with a cryostat (Leica CM3050S, Leica Biosystems, Buffalo Grove, IL, USA), and collected in individual wells. Representative free-floating sections from EC-Tau and littermate control mice at 30+ month of age were stained with human specific, anti-tau antibodies MC1 or CP27 (courtesy of Dr. Peter Davies; 1:500), mouse/human AT8 or AT180 (Thermo Scientific, Rockford, IL, USA; 1:500). In addition, every 9th free-floating sections from 30+ mo EC-Tau and control mice (n = 5 mice per group, 10 sections each mouse) starting from Bregma -2.04 mm to Bregma -4.88 mm were selected and stained with mouse NeuN antibody (EMD Millipore, Billerica, MA, USA; 1:1000), which is a specific neuronal marker.

Immunostaining was performed as previously described (Liu et al., 2012; Khan et al., 2014). In brief, free-floating mouse brain sections were blocked in 1.5% $H_2O_2$ (Fisher Scientific) in PBS for 10 min, and incubated with the above appropriate primary antibody in PBS containing 0.3% Triton X-100 (Sigma-Aldrich) (PBST) and 5% normal goat serum (Vector Laboratories, Burlingame, CA, USA) at 4°C overnight. After three washes with PBST, the sections were incubated with SuperPicture horseradish peroxidase (HRP) polymer conjugate Broad spectrum (Invitrogen, Frederick, MD, USA) for 15 min at room temperature on a rotator. Following three washes with PBS, immunoreactive material was visualized using

3,3′-diaminobenzidine tetrahydrochloride (DAB) (Sigma-Aldrich) as chromagen. The stained sections were mounted on slides and inspected by light microscopy (Olympus BX50, Olympus, Center Valley, PA, USA).

A semiquantitative count of NeuN-positive neurons in the EC-II and EC-III/IV was performed in selected sections from 5 control and 5 EC-Tau mice. For each mouse, a total of 10 NeuN-stained horizontal sections starting from Bregma -2.04 mm, spaced at ~300 μm, were included for automated cell counting (http://imagej.net/Particle_Analysis) using the ImageJ software (version 1.48, US National Institutes of Health, Bethesda, Maryland, USA).

## Morris water maze (MWM) tests

Spatial learning and memory was assessed using the MWM test including hidden platform acquisition and probe trial test. All the tests were automated and recorded using ANY-maze video tracking software (Stoelting Co., Wood Dale, IL, USA). Briefly, mice (n = 10 controls and 9 EC-Tau mice at 14 mo; n = 7 controls and 7 EC-Tau mice at 30+ mo) were tested in a cylindrical tank of 120 cm in diameter and 60 cm in height. The tank was filled with water at around 25 °C made opaque by adding Palmer Prism tempera white paint (Palmer Paint Products, Troy, Michigan, USA) until the platform was submerged 1.5 cm below the water surface. The tank was divided into four quadrants with different navigation landmarks for each quadrant. The midpoint of the wall in each quadrant was used as the starting location from where animals were released into the water.

In the hidden platform acquisition test, mice were allowed to swim freely to search for the escape platform within a maximum of 60 s. The platform location remained constant throughout the test. The time taken to reach the platform was recorded as the escape latency. The mouse was kept on the platform for 10 s after it found the hidden platform. If a mouse failed to find the platform within 60 s, it was guided to the platform and placed on the platform for 10 s; in this case, the escape latency was recorded as 60 s for this trial. The same animal was released from a new starting quadrant 4 min after the previous trial. The experiment was repeated with 6 trials per mouse each day and 4 consecutive days. The mean escape latency was measured to evaluate the spatial learning ability.

Two hours and twenty-four hours after the hidden platform acquisition test, probe trials were conducted by removing the platform. Mice were placed in the diagonal quadrant of the hidden platform originally located and were allowed to swim freely in the pool for 60 s. The number of entries into the area around the original hidden platform, i.e. the number of crossings over the previous platform location, was used to indicate the short-term and long-term memory maintenance.

At the end of the 24 h probe trial, a colorful flag was placed on the top of the hidden platform, which was opposite to the testing quadrant. The mouse was released at three different quadrants, and the time spent to find the flag was recorded as a measure of visual ability. All of the MWM tests were performed by two experienced technicians who were blind to the genotype of the animals.

### T-maze spontaneous alternation

Mice (n = 10 controls and 9 EC-Tau mice at 14 mo; n = 8 controls and 8 EC-Tau mice at 30 mo) were tested for spontaneous alternation on a T-shaped maze as previously described (Deacon and Rawlins, 2006). We used a spatial T-maze which had a black cue card on the left side of the stem. After one-day habituation, mice were first placed at the stem of the T-maze [measured 40 (stem) × 46 (arm) × 10 (width) cm] and allowed to choose to explore one open goal arm of the maze for 30 s throughout a twelve-trial continuous alternation sessions. Once a goal arm was chosen, the mouse was placed in the stem of the maze again, facing away from the goal arms, and the trial was repeated. The inside of the T-maze was wiped with 70% ethanol between different animal trials. For each animal, number of correct and incorrect choices were recorded in a contingency table. At the end of the experiment chi-square test was done to test statistical significance. All the tests were recorded by a technician blind to the genotype of the animals.

### Electrode implantation and surgery

Custom-made, reusable 16-channel microdrives (Axona, UK) were constructed as described previously by attaching an inner (23 ga) and an outer (19 ga) stainless steel cannula to the microdrives (Hussaini et al., 2011). Tetrodes were built by twisting four 25 mm thick platinum-iridium wires (California wires) and heat bonding them. Four such tetrodes were inserted into the inner cannula of the microdrive and connected to the wires of the microdrive. One day prior to surgery, the tetrodes were cut to an appropriate length and plated with a platinum/gold solution until the impedance dropped to about 150 ohms. On the day of surgery, mice were anesthetized with a mixture of ketamine and xylazine (100 mg/ml and 15 mg/ml, respectively, per 10 g body weight) and monitored for depth of anesthesia before proceeding. Mice were then fixed within the stereotaxic frame with the use of zygomatic process cuff holders and an incision was made to expose the skull. About 3–4 jeweler's screws were inserted into the skull to support the microdrive implant. An additional screw connected with wire was also inserted into the skull which served as a ground/reference for local field potential (LFP) recordings. A 2 mm hole was made on the skull at position 3.1 mm lateral to the midline and ~0.2 mm in front of the transverse sinus. Tetrodes were then lowered to about 0.8 mm from the surface of the brain (below dura) at an angle of 6-8$^{o}$ in the posterior direction in the sagittal plane. Dental cement was spread across the exposed skull and secured with the microdrive. Mice were allowed to recover from anesthesia in a cleaned cage placed on a warm heating pad until awake (~45 min) before finally being transported to housing. Carprofen (5 mg/kg) was administered to mice prior to surgery and post-operatively to reduce pain. Mice usually recovered within 24 h, after which the tetrodes were lowered and recording began. All recording depths reported are from the surface of the brain.

### *In vivo* recording and cell classification

The mice explored four alternating arenas during recording sessions: three white boxes (Box 1: 45 × 45 cm; Box 2: 55 × 55 cm; Box 3: 70 × 70 cm) or a white cylinder (dia. 70 cm). Twenty nine mice underwent two recording sessions per day, with ≥4 hr between sessions. For each new recording session, mice were exposed to either 1) a different arena than the

previous session, or 2) the same arena as the previous session, but with the arena and visual cue rotated. Tetrode positions were moved not more than 50μm at a time, and only after the last recording session of the day, allowing >12 hr of stable electrode positioning prior to the next recording session. All mice included in our study underwent ≥16 recording sessions, with the 30+ mo EC-Tau group having the highest number of sessions (1.3× more than age-matched control) to obtain similar overall cell numbers. Neuronal signals from experimental mice were recorded using the Axona DacqUSB system. The signals were amplified 15,000 to 30,000 times and band pass filtered between 0.8 and 6.7 kHz. LFP was recorded from 4 channels of the electrodes. The LFP was amplified 15,000 times, lowpass filtered at 125 Hz and sampled at 250 Hz. Notch filter was used to eliminate 60 Hz noise. The recording system tracked the position of the infrared LED on the head stage (sampling rate 50 Hz) by means of an overhead video camera. Position data were speed-filtered, only speeds of 3 cm/s or more were included. Tracking artifacts were removed by deleting samples greater than 100 cm/s and missing positions were interpolated with total durations less than 1 s, and then smoothing the path with a 21- sample boxcar window filter (400 ms; 10 samples on each side). Spike sorting was performed offline using TINT cluster-cutting software and Klustakwik automated clustering tool (Figure S2). The resulting clusters were further refined manually and were validated using autocorrelation and cross-correlation functions as additional separation tools. Quantitative measurements of cluster quality were subsequently performed, yielding isolation Distances in Mahalanobis space (Schmitzer-Torbert et al., 2005). There were no significant differences between clusters in our experimental groups (Median Isolation distances: 30+ mo EC-Tau- 10.40, 30+ mo control- 10.10, 14-mo EC-Tau- 9.46 and 14-mo control- 10.50. Kruskal-Wallis test- $P = 0.334$). A total of 434 excitatory neurons (122 grid cells, 93 head-direction (HD) cells, 22 border cells and 197 non-classified (NC) cells) and 93 interneurons were recorded from 29 mice for this study. There were four groups of mice and cell types for each group is as follows. Six 30+ mo EC-tau mice (26 grid; 26 HD; 5 border; 36 NC cells; and 22 interneurons), six 30+ mo control mice (30 grid; 15 HD; 7; border; 40 NC cells; and 22 interneurons), nine 14-mo old EC-tau mice (36 grid; 32 HD; 6 border; 78 NC cells; and 22 interneurons) and eight 14-mo old control mice (30 grid; 20 HD; 4 border; 43 NC cells; and 27 interneurons). There was no significant difference between the number of cells recorded within the two age groups. T-test between 30+ mo EC-Tau vs 30+ mo Control group: Grid cell- $P = 0.6658$, $t = 0.4450$, $df = 10$; Head-direction cells- $P = 0.2198$, $t = 1.309$, $df = 10$; Border cells- $P = 0.4608$, $t = 0.7670$, $df = 10$; Interneurons- $P = 1$, $t = 0.000$, $df = 10$ and NC cells- $P = 0.6658$, $t = 0.4450$, $df = 10$. T-test between 14-mo EC-Tau vs 14-mo Control group: Grid cell- $P = 0.8664$, $t = 0.712$, $df = 15$; Head-direction cells- $P = 0.4228$, $t = 0.8241$, $df = 15$; Border cells- $P = 0.6804$, $t = 0.4201$, $df = 15$; Interneurons- $P = 0.4366$, $t = 0.7993$, $df = 15$ and Mann Whitney $U$ test for NC cells- $P = 0.3836$, $U = 26.50$. Also, relative proportion of interneurons with respect to other excitatory cell types was not significantly different for 30+ mo group (EC-Tau: 19.84% and Control: 20.50%, $T$-test: $P = 0.8772$, $t = 0.1586$, $df = 10$) and 14-mo group (EC-Tau: 17.29% and Control: 22.73%, $T$-test: $P = 0.4650$, $t = 0.498$, $df = 15$). Note that the relative proportion of cells are the same across groups after increased recording sessions in the 30+ EC-Tau group. Head direction and border cells were identified as described previously (Bonnevie et al., 2013; Langston et al., 2010). Cells were classified as head-direction cells if they preferentially displayed tuning towards a particular direction in polar plots, while

border cells were identified by their characteristic firing fields in the proximity of an environmental boundary. All other MEC cells sampled that did not exhibit spatial preference or directional tuning were identified as non-classified cells. Putative excitatory cells were distinguished from putative interneurons based on waveform width (> 350 μs) and firing rate (< 30 Hz).

### Grid cell analysis and local field potentials

Firing rate distributions were determined by counting the number of spikes in each 2.5 cm × 2.5 cm bin as well as the time spent per bin. Maps for number of spikes and time were smoothed individually using a quasi-Gaussian kernel over the surrounding 5 × 5 bins. Analysis of grid cells was done as described previously (Bonnevie et al., 2013; Langston et al., 2010). Firing rates were determined by dividing spike number and time for each bin of the two smoothed maps. The peak rate was defined as the rate in the bin with the highest rate in the firing rate map. The structure of the rate maps was evaluated for all cells with more than 100 spikes by calculating the spatial autocorrelation for each smoothed rate map. The degree of spatial periodicity (grid scores) was determined for each recorded cell by taking a circular sample of the autocorrelogram, centered on the central peak but with the central peak excluded, and comparing rotated versions of this sample. Only cells that yielded positive grid scores were used for further analysis. To break the correlation between the firing pattern and animal's position, the data was shuffled 100 times by randomly shifting the spike times of each grid cell less than 20 seconds or more than 20 seconds relative to animal's position. Shuffling was done on the entire population of putative grid cells in the same age group and the same brain region (Figure S3A). Grid cells were defined as cells in which rotational symmetry based grid scores exceeded the 95$^{th}$ percentile of a distribution of grid scores for shuffled data. Out of 170 putative grid cells only 122 cells exceeded the 95$^{th}$ percentile criteria of 0.21. 76.9% of 14-mo control, 73.5% of 14-mo EC-Tau, 73% of 30+ mo control and 64% of 30+ EC-Tau cells passed the 0.21 threshold. Information content and spatial coherence was calculated as described previously (Hussaini et al., 2011). Spatial coherence estimates smoothness of a place field. It was calculated by correlating the firing rate in each pixel with firing rates averaged with its neighboring 8 pixels. It measures the extent to which the firing rate in a pixel is predicted by the rates in its neighbors (Muller and Kubie, 1989). Abrupt changes in firing rates of neighboring pixels make the place fields incoherent. Spatial information content is a measure used to predict the location of an animal from the firing of a cell. Information content was calculated using Skaggs' formula (Skaggs, 1993) and measures the amount of information carried by a single spike about the location of the animal and is expressed as bits per spike:

$$\text{Spatial information content} = \sum Pi \left(\frac{Ri}{R}\right) \log 2 \left(\frac{Ri}{R}\right)$$

Where: i is the bin/pixel number, Pi is the probability for occupancy of bin i, Ri is the mean firing rate for bin/pixel i and R is the overall firing mean rate. Head direction and border cells were identified as described previously (Bonnevie et al., 2013; Langston et al., 2010). Analysis of LFPs was done using EEGLAB (a toolbox for MATLAB) (Delorme and

Makeig, 2004). Briefly, log mean spectra of LFPs were calculated and percent distribution of power was calculated for theta (4-12 Hz) and gamma (35-55 Hz) frequency range (Hussaini et al., 2011). LFP analysis was speed filtered between 5-25 cm/sec to exclude speed related theta or gamma increase. There was no significant difference between the overall running speeds of control mice vs the EC-Tau mice (data not shown). After the recording experiments were complete, all surviving animals were deeply anesthetized and perfused with 4% PFA solution. The brains were then extracted, placed in 4% PFA solution and shaken for 24 hrs at 4°C. The following day the brains were transferred to 30% sucrose solution and shaken at 4°C until they sunk to the bottom of the tube. Brains were frozen and sectioned (30 μm) using a cryostat and processed further for either immunohistochemistry (explained below) or to identify tetrode tracts where visible, into the MEC (Figures S3C-D).

### Immunofluorescence

Free-floating brain sections were prepared in the same way as for immunohistochemistry. Sections (2 sections with 100 μm intervals from each mouse) were blocked in PBST containing 5% normal goat serum for 30 min at room temperature, and incubated with rabbit anti-TBR1 (Abcam, Cambridge, MA, USA; 1:500), rabbit anti-Parvalbumin (Thermo Scientific; 1:2000) or rat anti-Somatostatin (EMD Millipore; 1:100) antibody in PBST containing 5% normal goat serum at 4$^{o}$C overnight. After three washes with PBST, the sections were incubated with Alexa Fluor 594 goat anti-rabbit or Alexa Fluor 647 goat anti-rat IgG (Life Technologies, Grand Island, NY, USA; 1:1000) for 1 h at room temperature on a rotator. After three washes with PBST, the sections were blocked and incubated with antibody MC1 (1:1000) in PBST containing 5% normal goat serum at 4°C overnight. After three washes with PBST, the sections were incubated with Alexa Fluor 488 goat anti-mouse IgG (Life Technologies; 1:1000) for 1 h at room temperature. Following three washes with PBS, autofluorescence was quenched with 0.3% Sudan black in 70% ethanol (Decon Laboratories, King of Prussia, PA, USA) for 6 min at room temperature. The sections were rinsed with 70% ethanol and washed three times with 0.02% Tween-20 in PBS. The nuclei were stained with 5 μg/ml Hoechst33342 (Sigma-Aldrich) in PBST for 10 min at room temperature. Following three washes with PBS, sections were mounted on slides using SlowFade gold anti-fade reagent and imaged using confocal laser scanning microscopy via Z-stack. The number of TBR1$^{+}$, PV$^{+}$ or SOM$^{+}$ neurons in the MEC was quantified automatically using ImageJ.

## Quantification and Statistical Analysis

Prism 4 software (GraphPad, San Diego, CA, USA) was used to analyze the data. All the data are expressed as mean ± the standard error of the mean (SEM). We performed the D'Agostino & Pearson omnibus normality test to determine if the data was normally distributed. We then chose the following statistical tests. A two-way repeated measures ANOVA with Bonferroni post-tests was used to compare the escape latency and swim speed in 4 days of continuous hidden platform trials in MWM, as well as to compare power distributions of LFPs. The unpaired *t*-test was used to compare the number of platform crossings in 2 h and 24 h probe trials in the MWM. We used the Kruskal-Wallis test to compare median isolation distances in all groups for cluster quality. A Chi-square test was

used to compare the binary data from the T-maze test. The non-parametric Mann-Whitney *U* test was used to compare: the number of $NeuN^+$ and $TBR1^+/PV^+/SOM^+$ neurons, visual ability, and body weight, as well as all single-unit recording data. A value of $P < 0.05$ was considered statistically significant for all measures. The "n" represents the number of animals in each group, unless specified otherwise. The exact values of n are indicated in figure legends, supplemental figure legends, and in the Method Details section.

## Data and Software Availability

### Resource for Cluster Analysis

BatchTINTV2 is a graphical user interface (GUI) created by our lab as an end-user friendly batch processing solution to complement Axona's new command line modification of TINT. BatchTINTV2 code is deposited to the GitHub repository (https://doi.org/10.5281/zenodo.200977).

## Supplementary Material

Refer to Web version on PubMed Central for supplementary material.

## Acknowledgments

We thank Dr. Peter Davies for providing tau antibodies. We would like to thank Vadim Frolov and Dr. Edvard I. Moser for generously providing Matlab scripts for grid score analysis and Dr. James Donnett for help with cluster analysis. We wish to thank Dr. Catherine Clelland for assistance with statistical analysis and for providing helpful comments on the manuscript. We also Mark McNulty, Peter Salamon, and Kyle Peter for help with microdrive construction. This work was supported by research grants from National Institutes of Health (R01NS074874 to K.E.D. and R01AG050425 to S.A.H and K.E.D.) and the Alzheimer's Association (New Investigator Research Grant, 2015-NIRG-341570 to S.A.H).

## References

Allison SL, Fagan AM, Morris JC, Head D. Spatial Navigation in Preclinical Alzheimer's Disease. J Alzheimers Dis. 2016; 52:77–90. [PubMed: 26967209]

Belforte JE, Zsiros V, Sklar ER, Jiang Z, Yu G, Li Y, Quinlan EM, Nakazawa K. Postnatal NMDA receptor ablation in corticolimbic interneurons confers schizophrenia-like phenotypes. Nat Neurosci. 2010; 13:76–83. [PubMed: 19915563]

Bonnevie T, Dunn B, Fyhn M, Hafting T, Derdikman D, Kubie JL, Roudi Y, Moser EI, Moser MB. Grid cells require excitatory drive from the hippocampus. Nat Neurosci. 2013; 16:309–317. [PubMed: 23334581]

Booth CA, Ridler T, Murray TK, Ward MA, de Groot E, Goodfellow M, Phillips KG, Randall AD, Brown JT. Electrical and Network Neuronal Properties Are Preferentially Disrupted in Dorsal, But Not Ventral, Medial Entorhinal Cortex in a Mouse Model of Tauopathy. J Neurosci. 2016; 36:312–324. [PubMed: 26758825]

Braak H, Braak E. Neuropathological stageing of Alzheimer-related changes. Acta Neuropathol. 1991; 82:239–259. [PubMed: 1759558]

Brandon MP, Bogaard AR, Libby CP, Connerney MA, Gupta K, Hasselmo ME. Reduction of theta rhythm dissociates grid cell spatial periodicity from directional tuning. Science. 2011; 332:595–599. [PubMed: 21527714]

de Calignon A, Polydoro M, Suarez-Calvet M, William C, Adamowicz DH, Kopeikina KJ, Pitstick R, Sahara N, Ashe KH, Carlson GA, et al. Propagation of tau pathology in a model of early Alzheimer's disease. Neuron. 2012; 73:685–697. [PubMed: 22365544]

Deacon RM, Rawlins JN. T-maze alternation in the rodent. Nat Protoc. 2006; 1:7–12. [PubMed: 17406205]

Delorme A, Makeig S. EEGLAB: an open source toolbox for analysis of single-trial EEG dynamics including independent component analysis. J Neurosci Methods. 2004; 134:9–21. [PubMed: 15102499]

Fyhn M, Molden S, Witter MP, Moser EI, Moser MB. Spatial representation in the entorhinal cortex. Science. 2004; 305:1258–1264. [PubMed: 15333832]

Giocomo LM, Hussaini SA, Zheng F, Kandel ER, Moser MB, Moser EI. Grid cells use HCN1 channels for spatial scaling. Cell. 2011; 147:1159–1170. [PubMed: 22100643]

Gomez-Isla T, Price JL, McKeel DW Jr, Morris JC, Growdon JH, Hyman BT. Profound loss of layer II entorhinal cortex neurons occurs in very mild Alzheimer's disease. J Neurosci. 1996; 16:4491–4500. [PubMed: 8699259]

Hafting T, Fyhn M, Molden S, Moser MB, Moser EI. Microstructure of a spatial map in the entorhinal cortex. Nature. 2005; 436:801–806. [PubMed: 15965463]

Harris JA, Koyama A, Maeda S, Ho K, Devidze N, Dubal DB, Yu GQ, Masliah E, Mucke L. Human P301L-mutant tau expression in mouse entorhinal-hippocampal network causes tau aggregation and presynaptic pathology but no cognitive deficits. PLoS One. 2012; 7:e45881. [PubMed: 23029293]

Hof PR, Bussiere T, Gold G, Kovari E, Giannakopoulos P, Bouras C, Perl DP, Morrison JH. Stereologic evidence for persistence of viable neurons in layer II of the entorhinal cortex and the CA1 field in Alzheimer disease. J Neuropathol Exp Neurol. 2003; 62:55–67. [PubMed: 12528818]

Hussaini SA, Kempadoo KA, Thuault SJ, Siegelbaum SA, Kandel ER. Increased size and stability of CA1 and CA3 place fields in HCN1 knockout mice. Neuron. 2011; 72:643–653. [PubMed: 22099465]

Igarashi KM. The entorhinal map of space. Brain Res. 2016; 1637:177–187. [PubMed: 26940561]

Jacobs J, Kahana MJ, Ekstrom AD, Mollison MV, Fried I. A sense of direction in human entorhinal cortex. Proc Natl Acad Sci U S A. 2010; 107:6487–6492. [PubMed: 20308554]

Jeong J. EEG dynamics in patients with Alzheimer's disease. Clin Neurophysiol. 2004; 115:1490–1505. [PubMed: 15203050]

Khan UA, Liu L, Provenzano FA, Berman DE, Profaci CP, Sloan R, Mayeux R, Duff KE, Small SA. Molecular drivers and cortical spread of lateral entorhinal cortex dysfunction in preclinical Alzheimer's disease. Nat Neurosci. 2014; 17:304–311. [PubMed: 24362760]

Kropff E, Carmichael JE, Moser MB, Moser EI. Speed cells in the medial entorhinal cortex. Nature. 2015; 523:419–424. [PubMed: 26176924]

Kunz L, Schroder TN, Lee H, Montag C, Lachmann B, Sariyska R, Reuter M, Stirnberg R, Stocker T, Messing-Floeter PC, et al. Reduced grid-cell-like representations in adults at genetic risk for Alzheimer's disease. Science. 2015; 350:430–433. [PubMed: 26494756]

Langston RF, Ainge JA, Couey JJ, Canto CB, Bjerknes TL, Witter MP, Moser EI, Moser MB. Development of the spatial representation system in the rat. Science. 2010; 328:1576–1580. [PubMed: 20558721]

Lee VM, Goedert M, Trojanowski JQ. Neurodegenerative tauopathies. Annu Rev Neurosci. 2001; 24:1121–1159. [PubMed: 11520930]

Lithfous S, Dufour A, Despres O. Spatial navigation in normal aging and the prodromal stage of Alzheimer's disease: insights from imaging and behavioral studies. Ageing Res Rev. 2013; 12:201–213. [PubMed: 22771718]

Liu L, Drouet V, Wu JW, Witter MP, Small SA, Clelland C, Duff K. Trans-synaptic spread of tau pathology in vivo. PLoS One. 2012; 7:e31302. [PubMed: 22312444]

Masdeu JC, Zubieta JL, Arbizu J. Neuroimaging as a marker of the onset and progression of Alzheimer's disease. J Neurol Sci. 2005; 236:55–64. [PubMed: 15961110]

Matsuo ES, Shin RW, Billingsley ML, Van deVoorde A, O'Connor M, Trojanowski JQ, Lee VM. Biopsy-derived adult human brain tau is phosphorylated at many of the same sites as Alzheimer's disease paired helical filament tau. Neuron. 1994; 13:989–1002. [PubMed: 7946342]

Montez T, Poil SS, Jones BF, Manshanden I, Verbunt JP, van Dijk BW, Brussaard AB, van Ooyen A, Stam CJ, Scheltens P, Linkenkaer-Hansen K. Altered temporal correlations in parietal alpha and

prefrontal theta oscillations in early-stage Alzheimer disease. Proc Natl Acad Sci U S A. 2009; 106:1614–1619. [PubMed: 19164579]

Moretti DV, Fracassi C, Pievani M, Geroldi C, Binetti G, Zanetti O, Sosta K, Rossini PM, Frisoni GB. Increase of theta/gamma ratio is associated with memory impairment. Clin Neurophysiol. 2009; 120:295–303. [PubMed: 19121602]

Moser EI, Kropff E, Moser MB. Place cells, grid cells, and the brain's spatial representation system. Annu Rev Neurosci. 2008; 31:69–89. [PubMed: 18284371]

Muller R, Kubie J. The firing of hippocampal place cells predicts the future position of freely moving rats. J Neurosci. 1989; 9:4101–4110. [PubMed: 2592993]

Polydoro M, Dzhala VI, Pooler AM, Nicholls SB, McKinney AP, Sanchez L, Pitstick R, Carlson GA, Staley KJ, Spires-Jones TL, Hyman BT. Soluble pathological tau in the entorhinal cortex leads to presynaptic deficits in an early Alzheimer's disease model. Acta Neuropathol. 2014; 127:257–270. [PubMed: 24271788]

Quirk MC, Sosulski DL, Feierstein CE, Uchida N, Mainen ZF. A defined network of fast-spiking interneurons in orbitofrontal cortex: responses to behavioral contingencies and ketamine administration. Front Syst Neurosci. 2009; 3:13. [PubMed: 20057934]

Santacruz K, Lewis J, Spires T, Paulson J, Kotilinek L, Ingelsson M, Guimaraes A, DeTure M, Ramsden M, McGowan E, et al. Tau suppression in a neurodegenerative mouse model improves memory function. Science. 2005; 309:476–481. [PubMed: 16020737]

Schmitzer-Torbert N, Jackson J, Henze D, Harris K, Redish AD. Quantitative measures of cluster quality for use in extracellular recordings. Neuroscience. 2005; 131:1–11. [PubMed: 15680687]

Schultz H, Sommer T, Peters J. The Role of the Human Entorhinal Cortex in a Representational Account of Memory. Front Hum Neurosci. 2015; 9:628. [PubMed: 26635581]

Siwek ME, Muller R, Henseler C, Trog A, Lundt A, Wormuth C, Broich K, Ehninger D, Weiergraber M, Papazoglou A. Altered theta oscillations and aberrant cortical excitatory activity in the 5XFAD model of Alzheimer's disease. Neural Plast. 2015; 2015:781731. [PubMed: 25922768]

Skaggs WE, McNaughton BL, Gothard KM, Markus EJ. An information-theoretic approach to deciphering the hippocampal code. Advances in Neural Processing Systems. 1993; 5:1030–1037.

Stam CJ. Use of magnetoencephalography (MEG) to study functional brain networks in neurodegenerative disorders. J Neurol Sci. 2010; 289:128–134. [PubMed: 19729174]

Stark E, Eichler R, Roux L, Fujisawa S, Rotstein HG, Buzsaki G. Inhibition-induced theta resonance in cortical circuits. Neuron. 2013; 80:1263–1276. [PubMed: 24314731]

Stranahan AM, Mattson MP. Selective vulnerability of neurons in layer II of the entorhinal cortex during aging and Alzheimer's disease. Neural Plast. 2010; 2010:108190. [PubMed: 21331296]

Yasuda M, Mayford MR. CaMKII activation in the entorhinal cortex disrupts previously encoded spatial memory. Neuron. 2006; 50:309–318. [PubMed: 16630840]

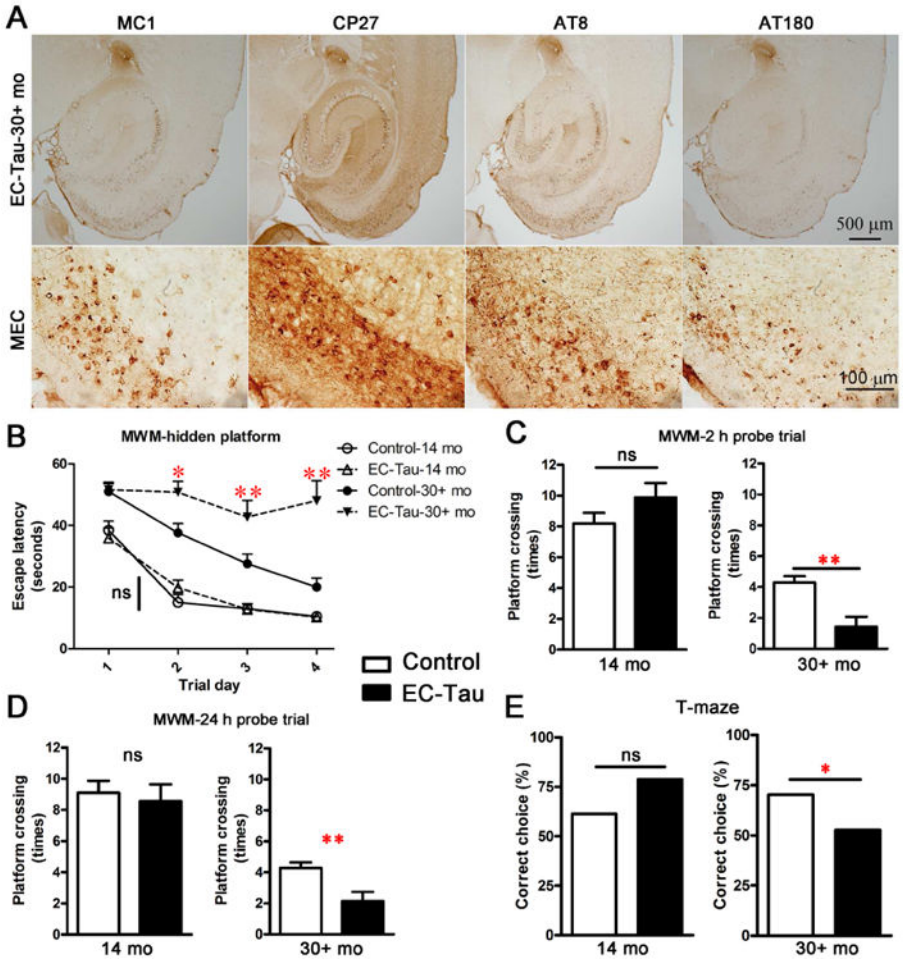


**Figure 1. Tau Pathology is Associated with Spatial Memory Deficits in Aged EC-Tau Mice**

(A) Tau pathology was identified in the EC and the hippocampal formation as well as in extrahippocampal areas of the cortex in 30+ mo EC-Tau mice. Sections from EC-Tau mice were stained with anti-tau antibodies (MC1, CP27, AT8 and AT180) and were developed using DAB as the chromagen. Tau immunoreactivity is indicated by brown staining. High magnification images of tau staining in the MEC are shown in the lower panel. (B-E) Spatial learning and memory deficits in aged EC-Tau mice. EC-Tau mice (n = 9 at 14-mo, 7 at 30+ mo) and littermate non transgenic controls (n = 10 at 14-mo, 7 at 30+ mo) were tested in the MWM (B-D) and T-maze (E). Data are expressed as mean ± the standard error of the mean (SEM). * $P < 0.05$ (EC-Tau 30+ mo *vs* Control 30+ mo on Trial Day 2 in (B), and EC-Tau 30+ mo *vs* Control 30+ mo in (E), ** $P < 0.01$ (EC-Tau 30+ mo *vs* Control 30+ mo on Trial Days 3-4 in (B), 2h Probe (C) and 24 h Probe (D)). A two-way repeated measures ANOVA with Bonferroni post-tests was used to compare the escape latencies in 4 days of continuous MWM hidden platform trials. Separate unpaired *t*-tests were used to compare the number of platform crossings in both 2 h and 24 h probe trials at 14-mo and 30+ mo. A chi-square test was used to compare the binary data (correct *vs* incorrect choice) from the T-maze test. See also Figure S1.

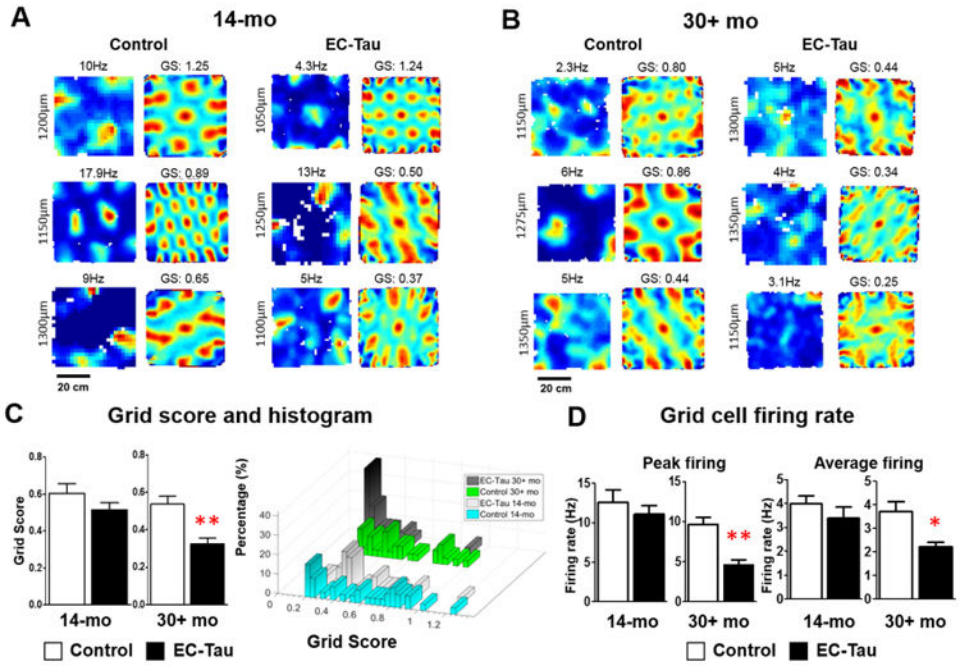


**Figure 2. Aged EC-Tau Mice Exhibit Reduced Grid Field Periodicity and Firing Rates**

(A-B) MEC grid cell firing rate maps and their autocorrelations are shown for 14-mo EC-Tau mice and 30+ mo EC-Tau mice along with age-matched controls. The representative firing rate maps were chosen to illustrate that grid scores appear to get worse with age as well as with increased tau accumulation. (A) Activity maps and autocorrelations were unchanged in the 14-mo EC-Tau mice compared to controls. (B) In contrast, activity maps and autocorrelations were severely affected in 30+ mo EC-Tau mice when compared to age-matched controls. Numbers on top and to the left of the activity maps indicate peak firing rate and recording depths from the surface of the brain, respectively. Numbers on top of the autocorrelation maps indicate grid scores (GS). Scale bars = 20 μm. (C) After applying an exclusion criterion of 95% (GS = 0.21) for shuffled grid scores, we found that grid cells from 30+ mo EC-Tau mice exhibit significantly reduced grid field periodicity compared to age-matched controls (30+ mo EC-Tau mice: GS=0.32, n=26 grid cells; 30+ mo control mice: GS=0.53, n=30 grid cells, $P < 0.0001$, Mann-Whitney $U$: 143.5). The group-wise histograms of observed grid score percentages across 122 grid cells show that the distribution for 30+ mo EC-Tau cells was shifted towards lower scores compared to other groups. (D) Peak firing rates and average firing rates of grid cells were reduced in 30+ mo EC-Tau mice when compared to age-matched controls (Peak Firing: 30+ mo EC-Tau mice: 4.5Hz, n=26 grid cells; 30+ mo control mice: 9.6Hz, n=30 grid cells, $P < 0.0001$, Mann-Whitney $U$: 127.5 and Average Firing: 30+ mo EC-Tau mice: 2.2Hz, n=26; 30+ mo control mice: 3.7Hz, n=30 grid cells, $P = 0.0161$, Mann-Whitney $U$: 243.0). All data are expressed as mean ± SEM. See also Figures S2, S3 and S5.

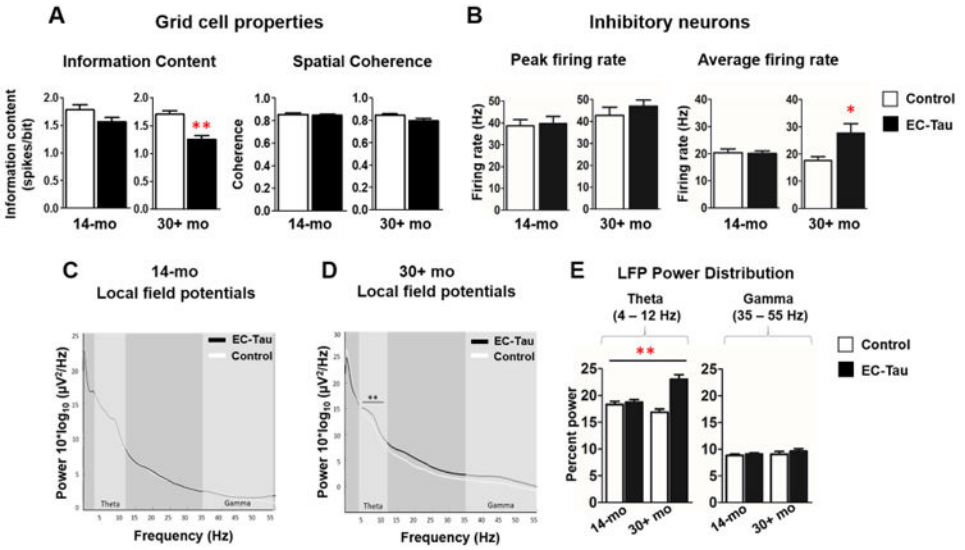


**Figure 3. Grid cell properties, Increased Interneuron Firing and Enhanced Power of Theta in the Dorsal MEC of Aged EC-Tau Mice**

(A) Left. Information content in the grid cells of 30+ mo EC-Tau mice was significantly reduced compared to aged-matched controls (30+ mo EC-Tau mice: Skaggs information content, 1.254; n=26 grid cells; 30+ mo control mice: Skaggs information content, 1.706; n=30 grid cells, $P < 0.0001$, Mann-Whitney $U$: 146.5). Right. There was no difference in grid cell spatial coherence in either group. (B) Putative interneurons show no difference in peak firing rates in mice at any age or genotype. However, interneurons of 30+ mo EC-Tau mice show increased average firing rates compared to age-matched controls (30+ mo EC-Tau mice: 27.7Hz, n=22 interneurons; 30+ mo control mice: 17.66Hz, n=22 interneurons, $P = 0.0193$, Mann-Whitney $U$: 142.5), while there was no difference in average firing rates in 14-mo animals. (C-D) Local field potentials (LFPs) were recorded from the MEC of (C) 14-mo and (D) 30+ mo mice. (E) Power distributions of LFPs in both 14-mo and 30+ mo mice are shown. The power in the theta range was significantly greater in 30+ mo EC-Tau mice compared to age-matched controls and 14-mo groups $^{**}P < 0.01$ (two-way ANOVA).

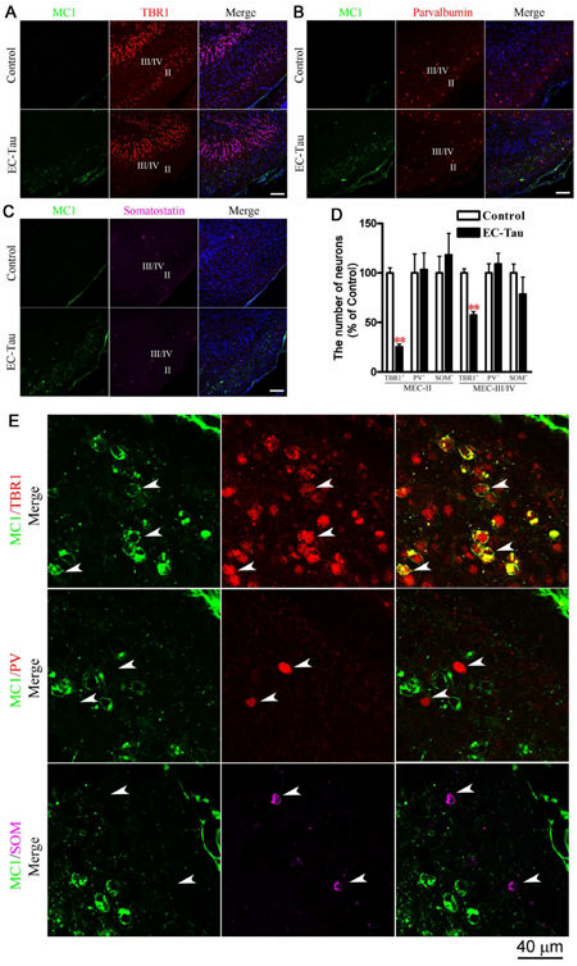


**Figure 4. The Number of Excitatory Neurons but not Inhibitory Neurons is Reduced in Aged EC-Tau Mice**

Sections from 30+ mo EC-Tau mice and age-matched controls were subjected to sequential staining with TBR1 (an excitatory neuronal marker) (A), Parvalbumin (PV, an inhibitory neuronal marker) (B) or Somatostatin (SOM, an inhibitory neuronal marker) (C) antibody, followed by incubation with the MC1 tau antibody. Scale bar = 100 μm. (D) The number of $TBR1^+$ excitatory neurons, but not $PV^+$ or $SOM^+$ inhibitory neurons were significantly reduced in MEC layers II and III/IV of 30+ mo EC-Tau mice (n = 8) compared to age-matched controls (n = 8). All data are expressed as mean ± SEM. ** $P < 0.01$ vs. control (non-parametric Mann-Whitney $U$ test). (E) Tau protein colocalized with excitatory neurons, but not inhibitory neurons in the MEC of aged EC-Tau mice. Sections were subjected to sequential staining with TBR1, Parvalbumin (PV) or Somatostatin (SOM) antibody, followed by incubation with MC1 tau antibody. $MC1^+$ tau staining was exclusively colocalized with $TBR1^+$ excitatory neurons, but not $PV^+$ or $SOM^+$ inhibitory neurons in the MEC of 30+ mo EC-Tau mice (n = 4). Scale bar = 40 μm. See also Figure S4.

## Key Resources Table

| Reagent or Resource | Source | Identifier |
|---|---|---|
| Antibodies | | |
| MC1 | Dr. Peter Davies | RRID: AB_2314773 |
| Mouse Anti-Phospho-PHF-tau pSer202/Thr205 Monoclonal Antibody, Unconjugated, Clone AT8 | Thermo Fisher Scientific | Cat# MN1020, RRID:AB_223647 |
| Mouse Phospho-PHF-tau pThr231 Antibody (AT180) | Thermo Fisher Scientific | Cat# MN1040, RRID:AB_223649 |
| Mouse Phospho-PHF-tau pThr212+Ser214 Antibody (AT100) | Thermo Fisher Scientific | Cat# MN1060, RRID:AB_223652 |
| Anti-NeuN, clone A60 antibody | Millipore | Cat# MAB377, RRID:AB_2298772 |
| TBR1 antibody | Abcam | Cat# ab31940, RRID:AB_2200219 |
| Parvalbumin antibody | Thermo Fisher Scientific | Cat# PA5-18389, RRID:AB_10977301 |
| Anti-Somatostatin, clone YC7 antibody | Millipore | Cat# MAB354, RRID:AB_2255365 |
| Experimental Models: Organisms/Strains | | |
| B6.Cg-Tg(Klk8-tTA)SMmay/MullMmmh | Mutant Mouse Resource Research Centers | RRID:MMRRC_0317 79-MU |
| FVB-Tg(tetO-MAPT*P301L)#Kha/JlwsJ | The Jackson Laboratory | RRID:IMSR_JAX:01 5815 |
| Software and Algorithms | | |
| ImageJ | NIH | RRID:SCR_003070 |
| ANY-maze | Stoelting Co. | RRID:SCR_014289 |
| EEGLAB | UCSD | RRID:SCR_007292 |
| GraphPad Prism | GraphPad | RRID:SCR_002798 |
| BatchTintV2 (Batch process Tint spike sorting) | GitHub | DOI:10.5281/zenodo .200977 |